Redesign and Simulation of MEMS Piezoelectric Microphone

Amir Amir Amir
123456@usn.no

Santosh Daggur Timmanna
266786@usn.no

Ismail Musa Hamid
277131@usn.no

Natnael Masresha Zerihun
277129@usn.no

Department of Microsystems
University of South-Eastern Norway Vestfold, Norway

***Abstract* — This study redesigns and simulates a circular membrane Piezoelectric MEMS microphone using COMSOL Multiphysics. The parameters were set to replicate a chosen design in a published paper as a reference model [1], using AlN as piezoelectric material. The model was then improved through geometry and by changing the piezoelectric material from AlN to ZnO and the passivation material from SiO_2 to Polyimide. This improvement increased the sensitivity from 1.1 mV/Pa to 3.21 mV/Pa. Customization of the resonance frequency of the membrane to around 4.87kHz enabled tuning the microphone model to Elk vocalization frequency in the range 100 to 3500 Hz.**

Keywords— MEMS microphone, Piezoelectric transduction, Aluminum nitride, COMSOL simulation.

I. INTRODUCTION

Microelectromechanical systems (MEMS) microphone is a transducer that converts acoustic pressure into electric output signal. MEMS microphones have revolutionized acoustic sensing, enabling compact, low-power solutions for consumer electronics, medical devices, and smart infrastructure. Despite their proliferation, conventional capacitive MEMS microphones face inherent limitations, including susceptibility to stiction-induced failures and performance degradation from off-chip CMOS integration, which introduces parasitic capacitances [2]. Piezoelectric transduction offers a compelling alternative, eliminating air-gap dependencies and external biasing while delivering linear, self-powered operation [3]. Compared to conventional capacitive MEMS microphones, piezoelectric MEMS microphones provide some benefits, such as improved signal-to-noise ratio, increased sensitivity, and resilience in challenging conditions. These microphones use the piezoelectric effect, which is the creation of an electric charge in reaction to mechanical stress, to detect sound effectively and precisely.

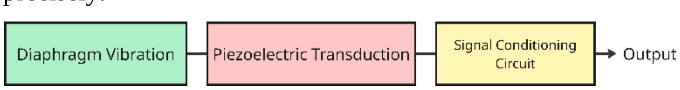

Fig. 1. Working Principle of MEMS Piezoelectric Microphone

The diaphragm of the microphone vibrates when sound waves enter the system. These vibrations are transformed into mechanical stress on the piezoelectric material. Piezoelectric material produces an electrical signal from mechanical stress. The circuit for signal conditioning transforms the electrical signal into a useful form. Output may be a storage device or audio processor that receives the signal after it has been processed.

Audio sensing and signal processing are two areas that have been greatly impacted by the quick development of MEMS technology. MEMS microphones have drawn a lot of interest among the different kinds of MEMS devices because of their small size, excellent performance, and integration potential. The redesign and simulation of a MEMS piezoelectric microphone, a particular kind of MEMS microphone that exploits the piezoelectric effect to transform sound waves into electrical signals, are the main topics of this study.

The selection of piezoelectric materials for MEMS microphones demands careful consideration of electromechanical coupling, fabrication compatibility, and noise characteristics. While PZT exhibits high piezoelectric coefficients ($d_{31} \approx 40$–70 pC/N), its high permittivity ($\varepsilon_{33} \approx 1700$) and low resistivity ($\sim 10^7 \Omega \cdot$ m) degrade signal-to-noise ratios (SNR) and bandwidth [1]. Conversely, aluminum nitride (AlN) emerges as a superior candidate due to its CMOS-compatibility, minimal dielectric loss ($\tan \delta = 0.002$), and high resistivity (10^{13}–10^{17} $\Omega \cdot$ m), attributes validated through Ashby and TOPSIS methodologies [4]. These properties mitigate parasitic effects and enhance sensitivity, positioning AlN as an ideal material for MEMS-CMOS integration [2]. Despite its superior characteristics, AlN has a lower piezoelectric coefficient which reduces its sensitivity. However, the piezoelectric coefficient can be improved by scandium doping or by increasing the thickness of the AlN layer.

This research addresses a specific gap in the literature regarding the optimization of piezoelectric MEMS microphones for enhanced sensitivity while maintaining low noise characteristics. Building on the monolithic piezoelectric microphone design by [1], this work employs COMSOL Multiphysics to simulate a circular AlN-SiO_2 membrane with optimized dimensions and electrode geometry. The study aims to validate analytical models predicting a resonance frequency of 11.2 kHz and an off-resonance sensitivity of 0.68 mV/Pa, while exploring design refinements to customize the frequency to our needs and increasing the sensitivity through geometry and material enhancement. By bridging computational modeling with experimental benchmarks, this analysis underscores the potential of piezoelectric MEMS microphones to address the escalating demands for high-fidelity, miniaturized acoustic sensors.

A. *Literature Review*

Piezoelectric MEMS microphones have gained considerable attention in recent years due to their intrinsic ability to convert mechanical pressure into electrical signals, offering advantages such as low power consumption, robust frequency response, and potential for CMOS integration. Fabrication techniques for these devices vary widely depending on the choice of piezoelectric material, structural architecture, and packaging constraints. This review highlights recent developments across three key dimensions: material systems, structural innovations, and processing techniques.

The standard fabrication flow begins with a silicon or silicon-on-insulator (SOI) wafer. A thin insulating layer, typically SiO_2 or Si_3N_4, is deposited via thermal oxidation or low-pressure chemical vapor deposition (LPCVD). Bottom electrodes such as Pt, Mo, or Au are then deposited using sputtering techniques. The piezoelectric film—commonly AlN, ScAlN, ZnO, or PZT—is applied through sputtering, sol-gel spin coating, or Metal-oxide Chemical Vapor Deposition (MOCVD). Top electrodes are patterned through photolithography and lift-off. Structural definition, including membrane or cantilever release, is achieved by wet etching (e.g., TMAH, KOH) or dry techniques like deep reactive ion etching (DRIE), often using the buried oxide in SOI wafers as an etch stop.

Several works have pushed the boundaries in terms of material innovation. Segovia-Fernandez et al. [1] developed a monolithic AlN-based microphone, compatible with CMOS processes, using Al-Ge eutectic bonding for wafer-level integration. Lu et al. [5] introduced $Sc_{0.2}Al_{0.8}N$ to improve piezoelectric response while maintaining thermal compatibility with standard processes. A more advanced approach was proposed by You et al. [6], who used single-crystal PZT and incorporated rib structures to improve mechanical sensitivity and structural integrity.

Structural design plays a critical role in performance. Chen et al. [7] fabricated patterned unimorph cantilevers with PZT films to enhance signal-to-noise ratio (SNR). Liu et al. [8] developed a resonant ZnO-based cantilever array tailored for respiratory sound acquisition. Lu et al. [5] further advanced this approach by adding a suspended proof mass, which amplifies low-frequency signal response through inertial enhancement.

Alternative approaches have also prioritized cost reduction and simplicity. Sawane et al. [9] replaced conventional piezo deposition with a pre-fabricated Ag/PZT/Ag diaphragm bonded via silver epoxy, eliminating high-temperature steps. Similarly, Ali and Prasad [10] fabricated a ZnO-based microphone using bulk micromachining with TMAH and anodic bonding to Pyrex glass, streamlining the release and packaging stages.

Despite diverse innovations, uniting low-cost processing and CMOS compatibility, high sensitivity remains an open challenge. The monolithic AlN-CMOS strategy [1] appears promising, offering an efficient integration route for high-performance, scalable acoustic sensing systems.

II. Model Description

The model is developed in COMSOL Multiphysics using a 2D axisymmetric geometry to reduce computational costs while accurately capturing the physical behavior of the circular diaphragm. The simulation focuses on the membrane's deformation under pressure loading and the resulting electrical output.

A. *Physics*

Initially, we planned to fully couple three physics domains: Solid Mechanics (for mechanical deformation), Electrostatics (for voltage generation through piezoelectricity), and Pressure Acoustics (for modeling sound wave pressure on the membrane through the surrounding air). However, to simplify the model during the development phase, temporarily disabled the Pressure Acoustics module and instead applied a boundary load directly within the Solid Mechanics interface to approximate the acoustic pressure.

Solid Mechanics interface of COMSOL Multiphysics is deployed to model the mechanical deformation of the multilayered membrane under applied pressure, enabling the analysis of stresses, strains, and deflections within the structure. To capture the electromechanical coupling behavior, the Electrostatics interface with the piezoelectric effect enabled is used to solve the electric potential generated due to mechanical deformation. These two physics interfaces are coupled using the Piezoelectric Effect Multiphysics coupling, which allows for the accurate simulation of the interaction between mechanical stress and electric field in the piezoelectric layers.

In future work, we plan to extend this study by incorporating the Pressure Acoustics, Frequency Domain module to model interactions with the surrounding air and background acoustic fields.

B. *Model Geometry, Materials, and Mesh*

The modeled MEMS microphone structure replicates the materials and design outlined in the reference study [1], employing standard materials in MEMS fabrication to ensure both high fidelity and performance. The 3D membrane structure shown in Fig. 2 comprises four main functional layers: a passive insulating layer, a piezoelectric layer, and two electrodes. Fig. 3 highlights the cross-sectional part in the membrane that has been modeled in COMSOL using axial symmetry, while its resultant geometry is shown in Fig. 4.

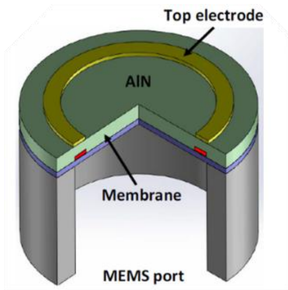

Fig. 2. Illustration of the circular-shaped piezoelectric microphone with the outer ring electrode [1]

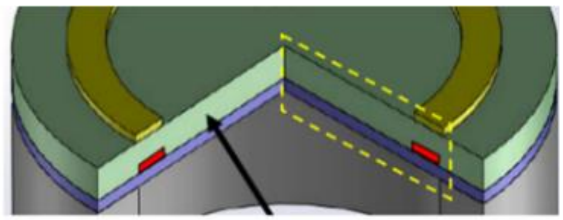

Fig. 3. Cross-sectional view of the membrane

The first layer from the bottom is silicon dioxide (SiO_2), providing both mechanical support to the membrane and electrical isolation between active elements and the substrate. Positioned above it is the aluminum nitride (AlN) piezoelectric layer which serves as the active sensing material, converting mechanical pressure into an electrical signal through electromechanical coupling. The electrical contacts are formed by a top electrode of aluminum (Al) and a bottom electrode of molybdenum (Mo), located symmetrically on either side of the AlN layer.

Geometrically, the SiO_2 and AlN layers both have a radius of 800µm and a thickness of 1µm. The electrodes are comparatively thinner, each measuring 200 nm thick, equivalent to one-fifth the thickness of the piezoelectric layer. The electrode design features a ring-shaped active region near the membrane's outer edge, covering approximately 15% of the membrane area. Fig. 4 illustrates the composition and dimensions of the geometry built in COMSOL.

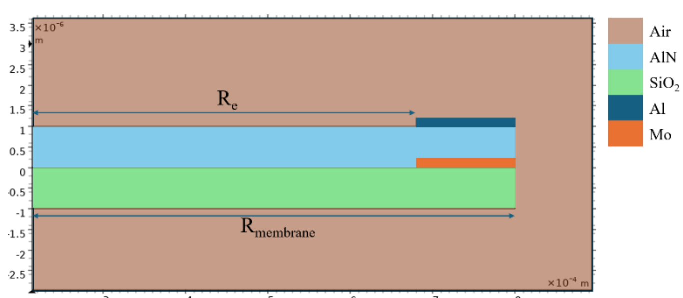

Fig. 4. Membrane Layers' Materials and Dimensions

Additionally, the surrounding air was modeled explicitly as a cylindrical volume enclosing the membrane to capture acoustic-structure interaction effects. The air domain, shown in Fig. 4, ensures accurate simulation of pressure wave propagation and the membrane's acoustic response.

The meshing strategy used free triangular elements with a finer element size applied to the whole geometry to accurately capture the deformation and electrical behavior. A moving mesh was applied to the air surrounding the membrane with a symmetric boundary relatively far from the device.

C. *Boundary Conditions*

1) *Mechanical Boundary Conditions*

The outer edge of the membrane (the boundary at the edge of the SiO2, AlN and Mo structural layers) was set as a Fixed Constraint to simulate clamping, while free deformation was allowed within the membrane's active region, as shown in Fig. 5.

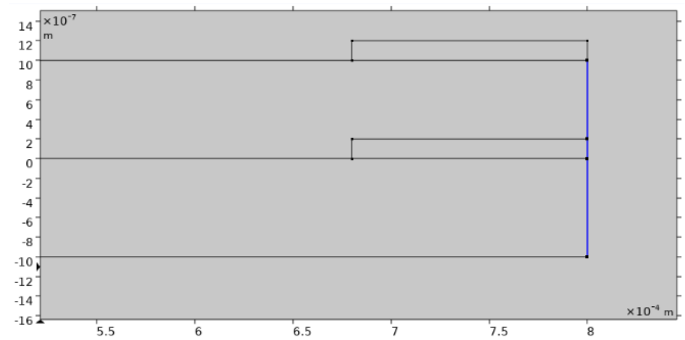

Fig. 5. The selected fixed constraint boundary in COMSOL indicated by a blue line

2) *Electrical Boundary Conditions*

The bottom electrode was assigned a Floating Potential boundary condition, allowing it to develop a natural voltage in response to mechanical loading. The top electrode was assigned as the reference electrode and set to ground (V=0 V).

The electrical output of the microphone was monitored by measuring the surface-averaged potential difference between the two electrodes under results, corresponding to the microphone's terminal voltage response.

D. *Loading Conditions*

A uniform pressure boundary load was applied to the top surface of the membrane (top boundary) to simulate incident acoustic pressure from the environment, as illustrated in Fig. 6. The mechanical loading approach varied depending on the specific simulation objective and the study being conducted.

Initially, for the Off-Resonance Sensitivity and Linearity tests, a sinusoidal pressure function was applied at a frequency far below the resonance region (1 kHz). Pressure sweeps were conducted from 0.5 Pa to 2 Pa for sensitivity evaluation, and from 0.1 Pa to 10 Pa for linearity assessment.

For the Frequency Response test, a constant amplitude pressure of 1Pa was applied, while the frequency was swept from 100 Hz to 12 kHz.

After customizing the sensor design, all the three loading cases were re-applied to the updated model, and the corresponding microphone output voltages were recorded for each study.

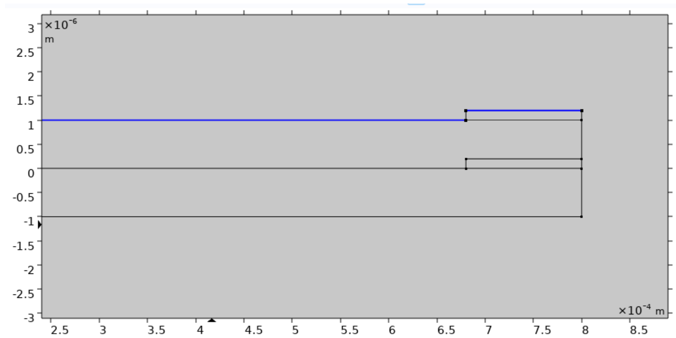

Fig. 6. Pressure boundary load applied to the top surface boundary of the membrane

E. Studies

Conducted two primary types of studies with one sub-study. Eigenfrequency Study, which identifies the membrane's natural vibration frequencies (fundamental modes), which helps predict the system's resonant behavior and mechanical bandwidth. It also allow us to observe how variations in parameters like radius, thickness, geometry and materials affect the operating frequency range. After modifying parameters, re-evaluated the natural frequency.

Frequency Domain Study: This study sweeps the input frequency over a specified range (i.e 200 Hz to 12500 Hz) to capture the frequency response of the membrane (floating potential vs. frequency). It identifies resonance peaks, determines the Q-factor, and extracts the half-power bandwidth.

Parametric sweep study is a sub-study of the two main studies and allows controlled variation of chosen parameters to observe system responses. We performed both single and combined parameter variations. Our parameters were structured for easy adjustment during studies. The key parameters are shown in Table 1 below.

Table 1. COMSOL PARAMETER LIST

Name	**Expression**	**Description**
R_membrane	800[µm]*factor_1	Total Membrane Radius
R_e	R_membrane*factor_2	Electrodes distance from center (Total radius - electrode width)
Electrode_width	R_membrane- R_e	Electrode width
T_piezolayer	1[µm]	Thickness of piezoelectric layer
T_SiO2	1[µm]	Thickness of SiO2 layer
T_electrode	0.2[µm]	Thickness of electrodes
P_in	1[Pa]	Applied pressure at the membrane
Air_dimension	20*R_membrane	Air dimension
factor_1	1	Ratio controlling membrane radius
factor_2	0.85	Ratio controlling electrode width

We varied and explored several design and operational parameters. Firstly, the membrane radius varied parametrically to study the effect of radius on resonant frequency. This helped us to replicate the results from our reference paper [1] as well as to improve the system eventually. Secondly, a parametric sweep of the boundary load pressure was conducted to validate that higher pressure on the membrane results in higher voltage output. For the frequency domain study, however, the operating pressure was fixed at 1Pa while varying the frequency. The sweep range was adjusted based on the expected resonance locations to ensure computational stability and capture detailed resonance behavior. Finally, we performed analysis of sensitivity by varying geometry such as electrode width and thickness of the passive and piezo layers.

To facilitate radius and electrode width variations, we introduced two scaling factors (factor_1 and factor_2) that multiply the desired base values, as shown in the parameter table above.

III. Results and Discussion

A. Theoretical Parameters and Equivalent Circuit Estimations

Some model parameters were calculated directly from the material properties. To calculate the resonance frequency, the flexural rigidity (D) and the mass per unit area (μ) were first determined. The resonance frequency was calculated using equation (1), yielding a value of 12.6 kHz.

$$\text{fr} = \frac{3.19^2}{2\cdot pi\cdot R^2}\cdot\sqrt{\frac{D}{\mu}} \qquad (1)$$

Another key parameter derived was the static capacitance (C_0), which depends on the permittivity, the thickness of the piezoelectric layer, the membrane radius, and the electrode coverage. C_0 is defined by equation (2), and was found to be 3.6 × 10^{-12} F.

$$C0 = \varepsilon_{r(AlN)}\cdot\varepsilon_r\cdot\frac{pi\cdot R^2}{t_{(AlN)}}\cdot\left(\frac{(R-Re)}{R}\right)^2 \quad (2)$$

An equivalent circuit of the model is shown in Fig. 7, with η being the electromechanical coupling coefficient. The acoustic package stiffness (K_p) is negligible. The parallel capacitance (C_p) is also a thousand times smaller than the purely electrical capacitance (C_o), hence neglected. This reduces the equivalent circuit to what is given in Fig. 8.

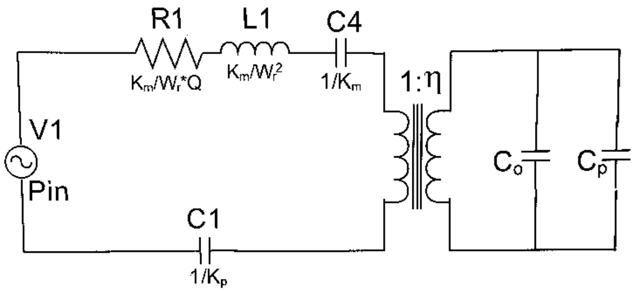

Fig. 7. Equivalent Circuit showing the electromechanical and acoustic parts.

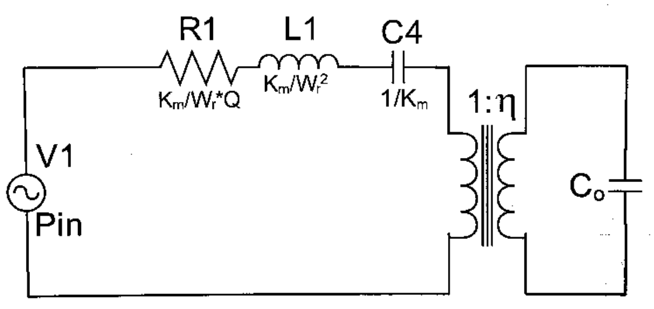

Fig. 8. Reduced Equivalent Circuit showing the electromechanical and acoustic parts

B. Paper Replication

1) Radius vs. Natural Frequency

To study the relationship between membrane radius and resonance behavior, a parametric sweep was performed by varying the membrane radius ($R_{membrane}$) from 500 µm to 1500 µm. The simulation results showed a clear decrease in the first-mode natural frequency with increasing radius. This trend is consistent with theoretical expectations, as the fundamental resonance frequency of a clamped circular membrane is inversely proportional to its radius. The simulated values are shown in Fig 9 (a), and they closely match the experimental data extracted from [1], presented in Fig. 9(b)

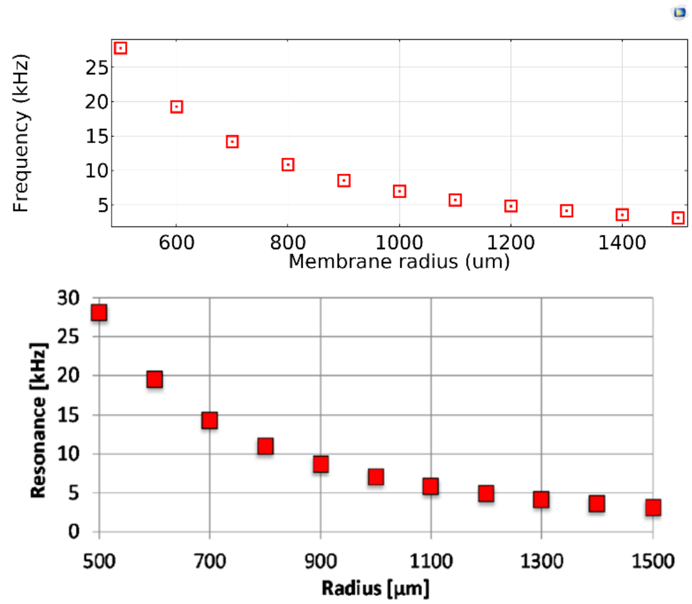

Fig. 9. Resonance frequency vs membrane radius (a) our COMSOL simulation (b) data from [1]

2) Sensitivity

To align with the baseline configuration presented in [1], a membrane radius of 800 µm was selected, with the electrode coverage set to 15% of the membrane radius. These parameters were held constant in the initial analysis. The microphone sensitivity was evaluated by either extracting the output potential at an input pressure of 1 Pa or by performing a parametric sweep of the input pressure (Pin) from 0.5 Pa to 3 Pa and then studying the rate or slope of the curve. A sensitivity of approximately 1.1 mV/Pa was obtained at 1 Pa. The results, presented in Fig. 10, compare the simulated data with the reference values reported in [1]. As shown, higher input pressures yielded a more pronounced output voltage, confirming the expected linear behavior within the small-signal regime.

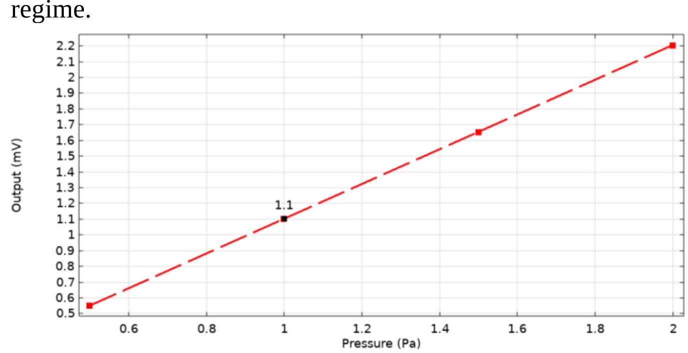

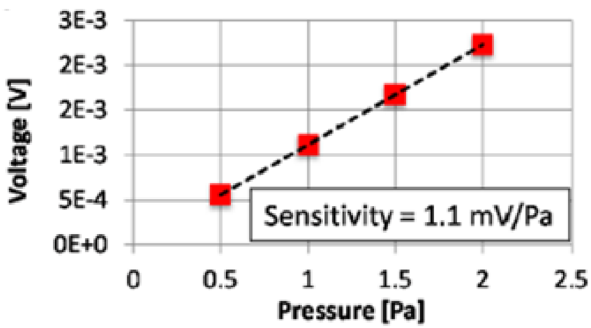

Fig. 10 Sensitivity Plot: input pressure vs output voltage (a) our COMSOL simulation (b) data from the reference [1]

3) Frequency Response

The frequency response of the system was examined to evaluate the microphone's behavior in both the linear and resonant regions. The resulting frequency response is shown in Fig. 11. Average sensitivity in the linear region was measured around 0.68, and the results were compared to those reported in [1]. As stated in [1], experimental values were approximately 38% lower than those predicted by COMSOL simulations (1.1 mV/Pa). To reflect this discrepancy, the COMSOL output voltage was scaled down by 38%, and the modified response is overlaid in Fig. 11. After adjustment, the simulated curve closely aligns with the experimental data reported in [1] which is shown in Fig. 12.

The response indicates that the microphone operates safely below its resonance frequency of approximately 11.2 kHz, with the primary working region situated well within the linear regime. The impact of future model modifications on off-resonance performance will be evaluated in subsequent studies.

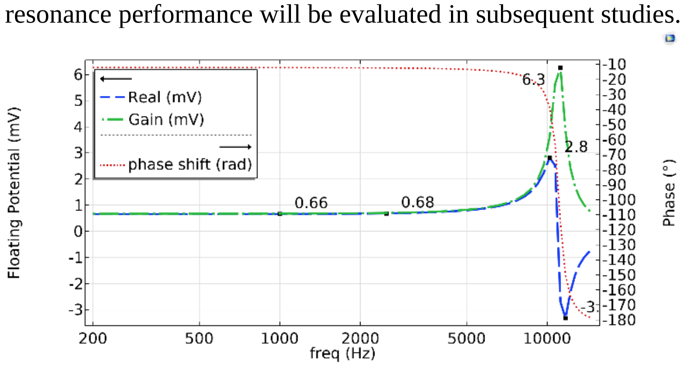

Fig. 11. frequency response of the system from our COMSOL simulation

The blue curve in Fig. 11 represents the real part of the floating potential and crosses zero due to phase inversion at resonance. This is expected, as the microphone behaves as a damped harmonic oscillator. The phase begins near 0° in the off-resonance region, transitions to approximately –90° at resonance, and approaches –180° at higher frequencies. The true gain amplitude (magnitude of the complex potential) is shown in green, representing the Bode amplitude response, while the red curve illustrates the phase shift in degrees. For comparison, the reference paper [1] only presents the real part of the potential, as shown in Fig. 12.

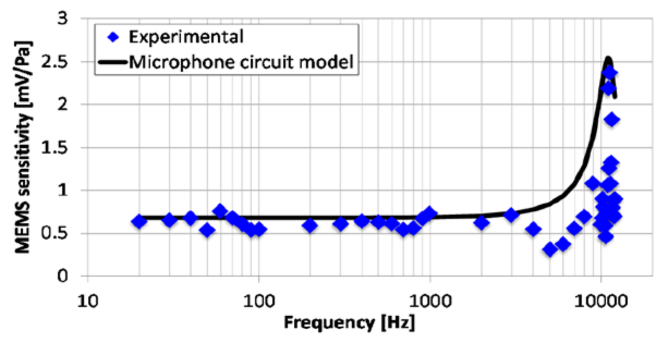

Fig. 12. frequency response of the system taken from [1]

4) Linearity

A linearity analysis was performed in COMSOL by sweeping input pressures from 0.1 Pa to 10 Pa, confirming that the microphone's sensitivity remains consistent across this range. This ensures accurate signal output that reflects the true intensity of incoming sound. The simulated curve aligns with the experimental data reported in [1] as the comparison is presented in Fig. 13. However, we scaled down the COMSOL output data by 38% because as mentioned earlier, the experimental values were approximately 38% lower than those predicted by COMSOL simulations.

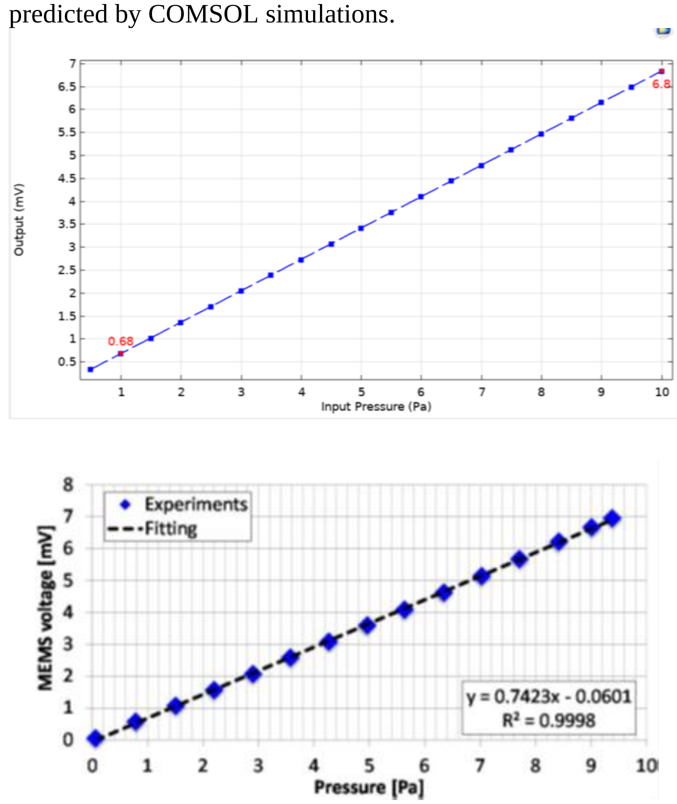

Fig. 13. linearity curve of the system (a)simulated with our model with 38% reduction (b) data from the reference paper[1]

C. Customization

Customized our model for Elk monitoring in its natural environment. To do so, we adapted the performance of the microphone to the specific acoustic characteristics of Elk vocalizations.

1) Target Frequency Range

Elk produces a range of vocalizations, with the most prominent sounds occurring in 100 to 3500 Hz frequency bands with priority given to the 200 to 2000 Hz band where the acoustic energy is strongest.

2) Sensitivity Requirements

To detect the signals of the animal reliably, the microphone minimum required sensitivity should be 3 mV/Pa or higher. The simulated design from the reference paper [1] provides a sensitivity of 1.1 mV/Pa, which is less than what is required for Elk monitoring, thus sensitivity improvement was needed.

D. Sensitivity Improvement Analysis

1) Materials

Polyimide was evaluated as a replacement for silicon dioxide (SiO_2) as the insulating layer. A sensitivity test was performed using both materials, and the comparison is shown in Fig. 14.

The use of polyimide improved the sensitivity due to its lower Young's modulus compared to SiO_2, which allowed greater membrane deflection and more effective stress transfer to the piezoelectric layer. However, while polyimide improves performance, it may present challenges in thermal and environmental stability compared to SiO_2, which should be considered during fabrication.

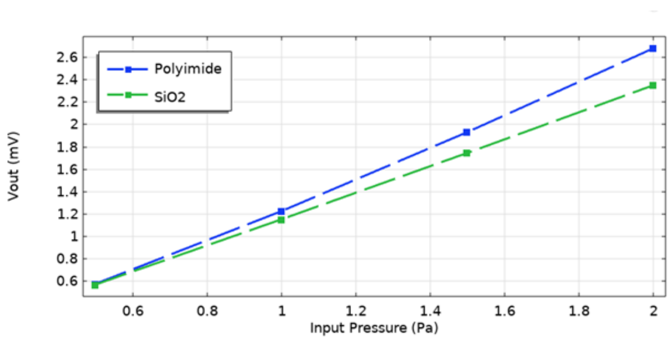

Fig. 14. Sensitivity curve comparison using SiO_2 and Polyimide as passivation layer

The sensitivity of the sensor was tested using different piezoelectric materials. Fig. 15 presents the resulting output voltages of the tested materials while sweeping the input pressure from 0.5 to 2 Pa. It can be clearly seen that ZnO is the material with highest sensitivity (2.68 mV/Pa) with excellent linearity (R^2= 0.999953). The comparison of the sensitivity for the tested materials at 1 Pa is shown in Fig. 16.

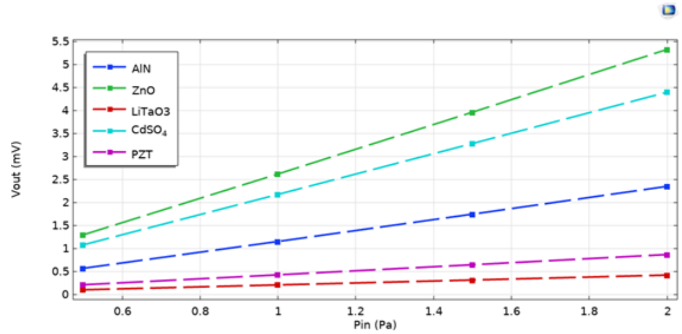

Fig. 15. Output curves using different piezoelectric materials

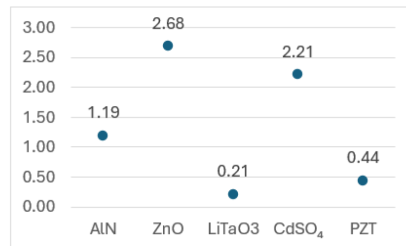

Fig. 16. The sensitivity of the microphone for each tested material in mV/Pa.

Moreover, multiple electrode materials were tested, and the combination of Aluminum (Al) as the top electrode and Molybdenum (Mo) as the bottom electrode yielded the best sensitivity performance in the model.

2) Geometry

The effect of the SiO_2 layer thickness on sensitivity was studied. Results showed an inverse relationship, thinner SiO_2 layers led to higher sensitivity, as depicted in Fig. 17. However, practical fabrication limitations impose constraints on minimizing this layer's thickness.

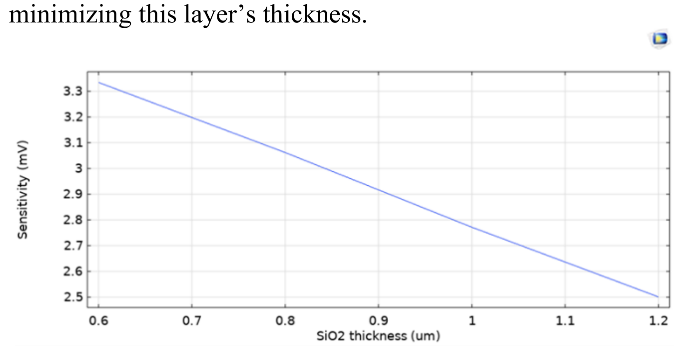

Fig. 17. effect of the thickness of SiO2 layer on sensitivity

It is found that the optimum thickness of AlN layer that gives the best sensitivity is 650 nm by sweeping the thickness and measuring the output voltage, as indicated in Fig 18.

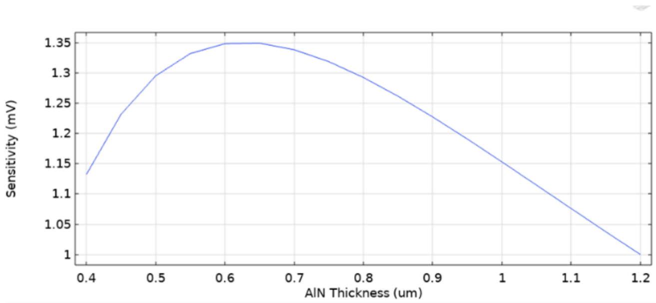

Fig. 18. Effect of the thickness of AlN layer on sensitivity

In addition to examining sensitivity as a function of pressure, the relationship between membrane radius and output voltage was also explored. The results indicated that sensitivity increases with membrane radius. Larger membranes produced higher output voltages at fixed pressure input. The influence of electrode width on sensitivity was also studied. It was found that reducing the electrode width and positioning the electrodes closer to the edge of the membrane led to improved sensitivity. These results are presented in Fig. 19.

While increasing the membrane radius and reducing the electrode width enhanced sensitivity, they introduced trade-offs. As previously discussed, a larger radius lowers the resonance frequency, which can reduce the usable linear frequency range of the microphone. Additionally, narrower electrodes present fabrication challenges, as thinner features increase process complexity, limit manufacturability and functionality.

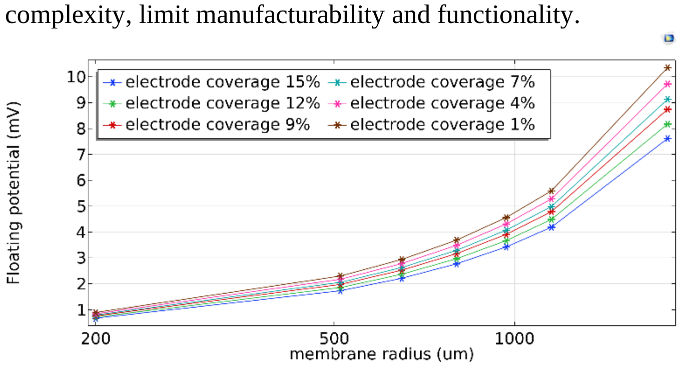

Fig. 19. membrane and electrode radius vs sensitivity Plot: lower electrode width gives high sensitivity

E. Final Customized Model

After evaluating the results of the sensitivity improvement, the piezoelectric material was changed to ZnO, while Polyimide was chosen as the membrane's passive layer. For geometry, the thicknesses of ZnO and Polyimide layers were set to 650 nm and 700 nm respectively. After changing the materials and setting optimal geometry to get the highest sensitivity an eigenfrequency study has been performed on the resultant model, Fig. 20, to choose the optimum radius. As shown in the figure, a radius of 600 um, corresponding to the 4.87 kHz resonance frequency, was chosen to suit our target frequency range and sensitivity needs.

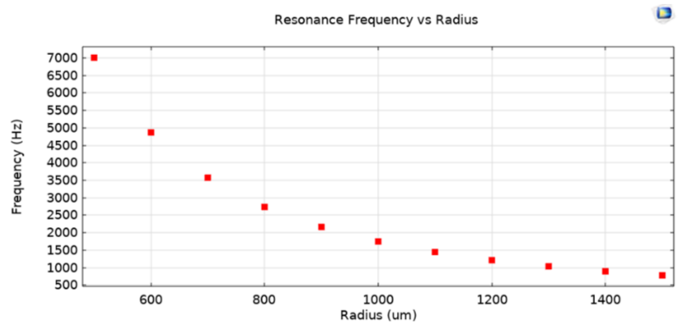

Fig. 20. Resonance Frequency Vs Radius for the final customized model

The same studies before the improvement were conducted for the final model and the output was plotted.

1) Sensitivity

After modeling, stationary sensitivity was obtained as 3.66 mV/Pa while off-resonance sensitivity at 1 kHz was about 3.21 mV/Pa as shown in Fig. 21. With new model parameters, the sensitivity of the revised model has been improved by a factor of three.

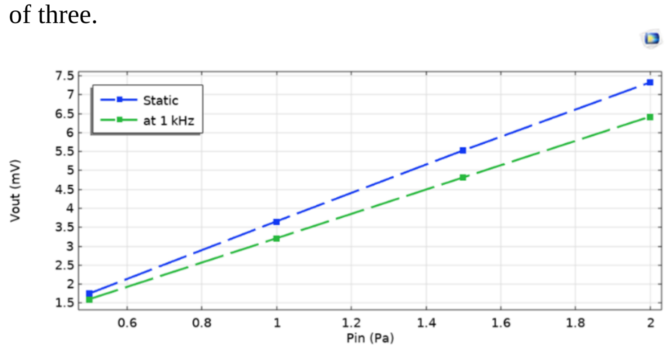

Fig. 21 Static and off-resonance Sensitivity for the improved model

2) linearity

A linearity study was done for input pressures from 0.1 Pa to 10 Pa at a constant 1 kHz frequency, which indicates that our model ensures a linear relationship between the output voltage of the microphone and the applied pressure on the membrane (coefficient of determination R^2= 0.999953). The linearity relation is illustrated in Fig. 22. Linearity is essential in giving an appropriate signal indicative of the sound that reaches the membrane. This prevents some sound signals from being overly loud or faint when they are not so in reality.

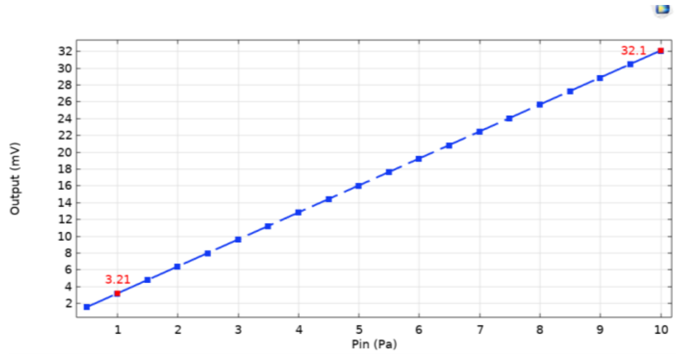

Fig. 22. linearity result for customized model

3) Frequency Response

The frequency response of the system was further evaluated after customizing the microphone design to better suit the intended application. As a result of the geometric and material changes in the membrane, the usable linear operating region shifted to lower frequencies. However, this modification led to a significant improvement in sensitivity within the linear range. Both the off-resonance and near-resonance behaviors of the customized system are illustrated in Fig. 23.

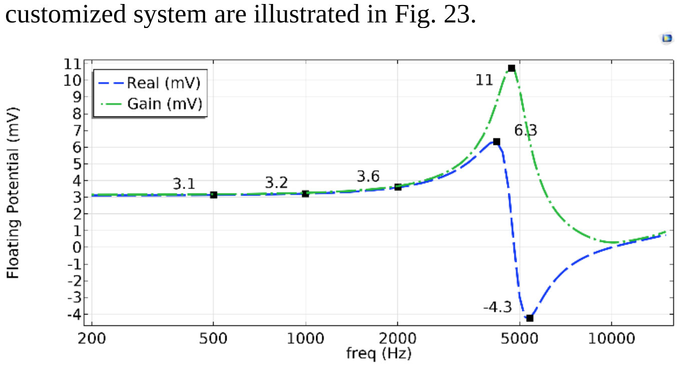

Fig. 23. frequency response of the system after customization

IV. CONCLUSION

In this work, we have successfully simulated and optimized a monolithic piezoelectric MEMS microphone using COMSOL Multiphysics. Through both analytical calculations and finite element simulations, we determined the resonance frequency characteristics of the original design. Initial simulations yielded a sensitivity of 1.1 mV/Pa, and the equivalent circuit model was established as depicted in Fig. 7.

Subsequently, we implemented strategic modifications to the microphone's geometry and material composition, resulting in a significant enhancement of the off-resonance sensitivity to 3.21 mV/Pa to nearly three times the original value. These customizations enabled the attainment of an operational frequency range spanning 0 to 4.87 kHz, which effectively encompasses the vocalization spectrum of Elks (100-3500 Hz). The modified design demonstrated excellent linearity in sensitivity with respect to applied pressure, confirming the robustness of our optimization approach.

Furthermore, we conducted a parametric analysis investigating the relationship between membrane radius and resonant frequency, for both the original and improved models. These analyses provide valuable design guidelines for frequency customization in similar piezoelectric MEMS microphone applications.

The enhanced sensitivity and precisely tailored frequency response achieved in this work demonstrate the effectiveness of our design for specialized acoustic sensing applications.

V. REFERENCES

[1] J. Segovia-Fernandez et al., "Monolithic piezoelectric aluminum nitride MEMS-CMOS microphone," Proc. IEEE Int. Conf. MEMS, pp. 1064–1067, 2016.

[2] W. Wang et al., "Design, fabrication and characterization of a high sensitivity MEMS capacitive microphone," Microsyst. Technol., vol. 20, no. 4, pp. 1029–1040, 2014.

[3] R. Littrell and K. Grosh, "Modeling and characterization of cantilever-based MEMS piezoelectric sensors and actuators," J. Microelectromech. Syst., vol. 21, no. 2, pp. 406–413, 2012.

[4] P. Gangidi and N. Gupta, "Optimal selection of dielectric film in piezoelectric MEMS microphone," Microsyst. Technol., vol. 25, pp. 4227–4235, 2019.

[5] L. Lu et al., “A piezoelectric MEMS microphone with proof mass and its array,” Microsyst. Technol., 2023.

[6] Z. You et al., “Piezoelectric MEMS microphones based on rib structures and single crystal PZT thin film,” Microsyst. Nanoeng., vol. 9, no. 1, 2023.

[7] Y.-C. Chen et al., “On the PZT/Si unimorph cantilever design for the signal-to-noise ratio enhancement of piezoelectric MEMS microphone,” J. Micromech. Microeng., vol. 31, no. 10, 2021.

[8] H. Liu et al., “MEMS piezoelectric resonant microphone array for lung sound classification,” J. Micromech. Microeng., vol. 33, no. 4, 2023.

[9] M. Sawane, M. Prasad, and S. Murugan, “Cost-effective fabrication of self-powered PZT based MEMS sensor for high sound pressure level measurement,” Microsyst. Technol., 2022.

[10] W. R. Ali and M. Prasad, “Design and fabrication of piezoelectric MEMS sensor for acoustic measurements,” Microsyst. Technol., 2022.

VI. DECLARATION

The authors of this project report wish to acknowledge that all listed authors contributed equally to the conception, literature review, and drafting of this manuscript. The order of authorship is alphabetical and does not reflect any hierarchical difference in contribution. Each author has provided substantial intellectual input and has approved the final version of the manuscript